

NUMERICAL SIMULATION OF A DEFORMABLE CELL IN MICROCHANNELS

F. NASON*, L. ZHU†, G. DUBINI* AND L. BRANDT†

* Department of Chemistry, Materials and Chemical Engineering "Giulio Natta"
Politecnico di Milano
P.za Leonardo da Vinci, 32 - 20133 Milano, Italy
e-mail: francesca.nason@mail.polimi.it

†Linne Flow Center and SeRC (Swedish e-Science Research Centre)
KTH Mechanics
Stockholm, Sweden
e-mail: luca@mech.kth.se

Key words: FSI, Coupled Problems, Single-cell, Computing Methods

Abstract. The main goal of this work is to numerically investigate the behavior of a cell flowing in a microfluidic system. In particular, we want to model flow-induced deformations of an isolated cell to quantitatively evaluate the cell response when subjected to a representative range of flow rates in a realistic geometry, with specific interest in the case of cell trapping. This research will help optimize operating conditions as well as the design of cell manipulation/culture micro-devices, so as to guarantee cell viability and ultimately improve high-throughput performance.

1 INTRODUCTION

To analyze, describe and also predict the motion of cells in large vessels, microcapillaries and cell separation devices, theoretical and computational models with various degrees of complexity and physiological relevance have been developed. In particular, in the context of particulate microhydrodynamics, cells are treated as capsules, defined as flexible particles formed by a well-defined, distinct, structured elastic membrane containing a liquid in the interior and possibly a stiff nucleus or core [12]. The hydrostatics and hydrodynamics of liquid capsules enclosed by thin elastic shells have therefore received considerable attention in cellular biology, bioengineering and even in microencapsulation technology [11]. The properties of the membrane material play a crucial role in the dynamics of the capsule, therefore the effect of the membrane mechanical properties on capsules shape at equilibrium, deformability and transient motion has been investigated in various types of simple flows. For a review of analytical, numerical and experimen-

tal works of the dynamics of capsules in shear flow the reader is referred to [10]. The effect of the interfacial elasticity on the capsule deformation and on the rheology of dilute suspensions for small deformations of the initial spherical shape were clarified by the pioneering theoretical investigations of Barthes-Biesel and Barthes-Biesel & Rallison [1, 2]. Numerical studies for moderate and large deformations were presented later, often together with experimental analyses. The effects of surface viscosity and incompressibility, relevant to biological membranes consisting of lipid bilayers, were considered more recently [10]. The analysis of the flow in the presence of a capsule is computationally very challenging. The kinematic and dynamic coupling of the flow enclosed in the capsule and the one surrounding it must account for the mechanical properties of the interface; moreover, an outstanding number of non-spherical transient shapes of the capsule can be obtained due to the membrane deformability and these must be computed simultaneously with the variables characterizing the flow [3].

In modern biology, a wealth of tools and new techniques are under development for cell analysis and in particular to investigate stem cells, as they represent a primary source of cells in the context of regenerative medicine [17]. It is believed that differentiated autologous stem cells would be the perfect inhabitants of an engineered tissue surrogate to be assembled and used surgically for bodily repair [14]. Microfluidics, due to its intrinsic characteristics and advantages, is commonly considered to be a powerful and enabling approach for studying cell behavior [15]. A plethora of evidence has shown that cellular heterogeneity commonly exists within an isogenic or clonal population. The most effective approach is therefore to analyze a population at individual cell level. However, a significant number of individual cells is required to obtain statistically meaningful data, and therefore high-throughput analysis is essential. Since cell populations can be very sensitive to stress, this must be taken into account when handling cell samples within high-throughput microfluidic devices, since high velocities may imply high shear stress acting on the cell membrane, potentially resulting in significant cell death and hence in a loss of representative sample across the initial population. [16]

The aim of this work is therefore to develop new state-of-art numerical tools to efficiently investigate the behavior of a cell flowing in a microfluidic system. After presenting our implementation, we simulate flow-induced deformations of an isolated cell run in a realistic microdevice.

2 MATERIALS AND METHODS

We investigate here the deformation of a cell flowing in a microchannel with a 90-degree bend, a configuration most likely to be encountered by cells loaded and run into a microfluidic device for cell culture, analytical purposes or cellular assays in general. To study the evolution of liquid capsules in microchannels we adopted a hybrid boundary integral/ immersed boundary method [13, 8], coupled with a spectral discretization of the membrane surface [18].

2.1 Fluid phase

For the fluid part, we solve the steady Stokes equation with boundary conditions given by the external walls limiting our domain and a forcing related to the internal stresses arising on the membranes

$$-\nabla p(\mathbf{x}) + \eta \nabla^2 \mathbf{u}(\mathbf{x}) + \boldsymbol{\rho}(\mathbf{x}) = 0 \quad (1)$$

$$\nabla \cdot \mathbf{u}(\mathbf{x}) = 0. \quad (2)$$

In the equation above $\boldsymbol{\rho}(\mathbf{x})$ represents point forces due to the deformable body in the flow. As mentioned above, these are related to the internal deformation of the suspended phase and will be described in detail in the following section. To solve the Stokes equation in a generally complex geometry we follow the General Geometry Ewald Method (GGEM) proposed by Graham [13, 8]. Exploiting the linearity of Stokes problem, we decompose the forcing as $\rho(x) = \rho_l(x) + \rho_g(x)$ where the local and global forcing read

$$\rho_l = \sum_{i=1}^n \mathbf{f}_i [\delta(\mathbf{x} - \mathbf{x}_i) - g(\mathbf{x} - \mathbf{x}_i)], \rho_g = \sum_{i=1}^n \mathbf{f}_i [g(\mathbf{x} - \mathbf{x}_i)]. \quad (3)$$

\mathbf{f}_i is the force density at the discrete points representing the effect of the membrane on the fluid and $g(r) = \frac{\alpha^3}{\pi^{3/2}} e^{(-\alpha^2 r^2)} [2.5 - \alpha^2 r^2]$ is a screen function used to decouple local and global solution.

The local solution $\mathbf{u}_l(\mathbf{x}) = \sum_{i=1}^n G_l(\mathbf{x} - \mathbf{x}_i) \cdot \mathbf{f}_i$ describes the near field effects of the forcing and does not account for any boundary effects or long range interactions. The Green function of the local problem can be computed analytically in free space

$$\mathbf{G}_l(\mathbf{x}) = \frac{1}{8\pi\eta} \left[\delta + \frac{\mathbf{xx}}{r^2} \right] \frac{\text{erfc}(\alpha r)}{r} - \frac{1}{8\pi\eta} \left[\delta - \frac{\mathbf{xx}}{r^2} \right] \frac{2\alpha}{\pi^{1/2}} e^{-\alpha^2 r^2} \quad (4)$$

with r the distance between the singularity and the evaluation point \mathbf{x} . In the numerical code, the solution at each grid point was obtained by summing only over the set of closest points. Indeed, the parameter α represents the scale of the screen function g and, as a consequence, it defines the length over which mutual interaction are taken into account (cut-off radius is chosen to be $4/\alpha$) as well as the grid size required for an accurate solution [8]. Note that $\mathbf{G}_l(x)$ is singular as $r \rightarrow 0$: two approaches can be followed here. i) Use singular integration as in traditional boundary integral methods [12, 13]; ii) regularized Stokeslet [7]. The second approach was followed for this work. The first approach turns out to be crucial for small confinement, small distances between walls and cell.

The global solution was obtained numerically as solution of the Stokes system (1) forced by $\rho_g(x)$ only. Boundary conditions at the solid boundaries are enforced such that the total solution $\mathbf{u} = \mathbf{u}_l + \mathbf{u}_g$ satisfies no slip.

The global Stokes problem can be addressed using any solver. In the present work, we adopted the open source Spectral Element Method (SEM) Nek5000 developed by Paul Fischer at Argonne National Laboratory, USA [5]. Nek5000 is a numerical code

for the simulation of steady and unsteady incompressible fluid flow and heat transfer, as well as optional convective-diffusive passive scalar quantities. The present method appears particularly suited for the numerical simulation of multiphase flow at vanishing Reynolds number in complex geometries. It combines the accuracy of the boundary integral approach and the flexibility of immersed boundary in terms of geometry. Possible extensions are described in [8]. To the best of our knowledge, we present here the first implementation of this method suited for any geometry.

2.2 Elastic membrane

To represent the surface of the cell we adopt spherical harmonics. Several advantages come when using this approach, such as the spectral accuracy and the solution of singularities at the poles when computing derivatives of the basis functions. In addition, this discretization provides uniform resolution over the surface ensuring minimum of the L_2 norm of the approximation error and removal of any time step limitation associated with the close spacing of the collocation points near the poles. Finally, dealiasing can be easily implemented to overcome nonlinear instability without degrading the accuracy of the solution.

The method shortly presented here closely follows the formulation in Zhao et al.[18]. The reader is referred to this paper for a more detailed description. The surface of each cell is represented as series of spherical harmonics function of the two angles $\theta \in [0, \pi]$ and $\phi \in [0, 2\pi)$

$$f(\theta, \phi) = \sum_{n=0}^{N-1} \sum_{m=0}^n \bar{P}_n^m(\cos \theta) (a_{nm} \cos m\phi + b_{nm} \sin m\phi) \quad (5)$$

with the orthonormal Legendre polynomial

$$\bar{P}_n^m(x) = \frac{1}{2^n n!} \sqrt{\frac{(2n+1)(n-m)!}{2(n+m)!}} (1-x^2)^{\frac{m}{2}} \frac{d^{n+m}}{dx^{n+m}} (x^2-1)^n \quad (6)$$

and N^2 the total number of spherical harmonics. Transforms are performed using the SPHEREPACK library.

Once the stress-free reference shape of the cell is defined, the surface deformation is described by the tensor $\mathbf{F} = \mathbf{a}_\alpha \mathbf{A}^\alpha$ mapping the curvilinear base vector in the undeformed state \mathbf{A}^α , into the current tangent vectors \mathbf{a}_α , $\alpha = 1, 2$. The local deformation is measured by the Cauchy–Green tensor $\mathbf{V}^2 = \mathbf{F} \cdot \mathbf{F}^T$ whose invariants are

$$I_1 = A^{\alpha\beta} a_{\alpha\beta} - 2, \quad I_2 = |A^{\alpha\beta}| |a_{\alpha\beta}| - 1,$$

where $|\cdot|$ defines the determinant of a matrix. To model a thin hyper-elastic membrane, two commonly used constitutive laws, the neo-Hookean law and the Skalak law are used. In the neo-Hookean model, the elastic strain energy W is written as

$$W = \frac{E_s}{2} \left(I_1 - 1 + \frac{1}{I_2 + 1} \right) \quad (7)$$

whereas, in the Skalak model, W is formulated as

$$W = \frac{E_s}{4} (I_1^2 + 2I_1 - 2I_2 + CI_2^2). \quad (8)$$

E_s is the elastic shear modulus and C is the reduced area dilation modulus. The first quantifies resistance to shear, whereas the second coefficient indicates resistance to area variations.

The contravariant expression for the in-plane stress tensor can be obtained as derivative of the elastic energy

$$\tau^{\alpha\beta} = \frac{2}{J_s} \frac{\partial W}{\partial I_1} A^{\alpha\beta} + 2J_s \frac{\partial W}{\partial I_2} a^{\alpha\beta}, \quad (9)$$

where $J_s = \sqrt{1 + I_2}$ indicates the ratio between deformed and undeformed surface area.

To be able to simulate conditions when negative tension occurs the bending stiffness of the membrane must be also taken into account. The bending moment was assumed to be linear and isotropic $M_\beta^\alpha = -E_B(b_\beta^\alpha - B_\beta^\alpha)$ where E_B is the bending modulus and B_β^α the curvature tensor for the reference state. The transverse force on the membrane Q^β can be obtained by a local torque balance

$$M_{|\alpha}^{\alpha\beta} - Q^\beta = 0, \quad (10)$$

where $\cdot_{|\alpha}$ is the covariant derivative. Finally, we impose force balance to derive an expression for the force density at the membrane

$$\tau_{|\alpha}^{\alpha\beta} - b_\alpha^\beta Q^\alpha + f^\beta = 0, \quad (\beta = 1, 2) \quad (11)$$

$$Q_{|\alpha}^\alpha + \tau^{\alpha\beta} b_{\alpha\beta} + f^3 = 0. \quad (12)$$

The numerical algorithm is as follows, where the Lagrangian mesh indicates the nodes used to discretize the membrane whereas the Eulerian mesh is used to solve the global Stokes problem.

1. Calculate analytically the local velocity $\mathbf{u}_l(\mathbf{x})$ on the Lagrangian mesh using the force density \mathbf{f} from the previous time step ($\mathbf{f} = 0$ at first time step).
2. Calculate the global velocity $\mathbf{u}_g(\mathbf{x})$ on the Eulerian mesh and interpolate onto the Lagrangian mesh.
3. Compute the total velocity $\mathbf{u}(\mathbf{x}) = \mathbf{u}_l(\mathbf{x}) + \mathbf{u}_g(\mathbf{x})$ and update the position of the Lagrangian points.
4. Compute the force density \mathbf{f} on the membrane surface.
5. Calculate the global forcing $\rho_g(x)$ on the Eulerian mesh and boundary conditions for next time step (item 2). The boundary conditions read $\mathbf{u}_g = \mathbf{u}_w - \mathbf{u}_l$, with \mathbf{u}_w prescribed at the wall.
6. Repeat from 1.

2.3 Nondimensionalization

We use Capillary number Ca to quantify the ratio between the viscous force and the elastic force. The definition of Ca varies for the two flow cases studied, namely, a capsule under constant shear flow and in plane Poiseuille flow for the 90-degree bend. For the first configuration, it is defined as $Ca = \frac{\eta \dot{\gamma} a}{E_s}$, where $\dot{\gamma}$, a and E_s are the flow shear rate, the cell radius and the surface shear elastic modulus. For the second configuration, $Ca = \frac{\eta \bar{U}}{E_s}$, where \bar{U} is the mean bulk velocity of the channel flow. Besides the reduced area dilation modulus C introduced in equation 8, we also introduce the reduced bending modulus C_B defined as $C_B = \frac{E_B}{a^2 E_s}$.

2.4 Grid and boundary conditions

To simulate a cell going through an L-bend, we impose the parabolic Poiseuille velocity profile at the inlet. To produce moderate confinement, the channel width is set to $3a$. As we focus on the effect of the deformation around the corner, no confinement is added in the spanwise direction: the length of the computational domain in this direction is set to $10a$, with periodic boundary conditions. We use uniform spectral elements to discretize the whole domain. Each element is subdivided into arrays of Gauss-Lobatto-Legendre (GLL) nodes for the velocity and Gauss-Legendre (GL) nodes for the pressure field. In our simulation, the size of each element is a and 4 GLL points are used in each direction. The length of the upstream and downstream channels is equal to $20a$ and the total number of velocity grid points is therefore 82560.

3 RESULTS

3.1 Code Validation

The code has been validated first against the data provided in [13]. In this work, the authors report the solution for the motion of liquid capsules under constant shear flow. Fluid viscosities inside and outside the capsule are matched, and a neo-Hookean model of the membrane elasticity is adopted, while the capsule bending stiffness is neglected. The results are presented in Fig. 1 a) in terms of capsule deformation measured by the Taylor parameter

$$D = \frac{L - B}{L + B} \quad (13)$$

where L and B denote the maximum and the minimum diameters in the shear plane of the ellipsoid of inertia of the deformed capsule. The code was also validated against the data provided by Huang et al. [6]. Here we do not consider pre-inflated capsule, but instead include a finite bending stiffness. Fig. 1b) reports the time evolution of the deformation for a capillary number $Ca = 0.15$. The maximum discrepancy between the solid line, our results, and the dotted like, taken from [6], is around 3%. Note however that Huang et al. consider small but finite Reynolds number while we solve the Stokes

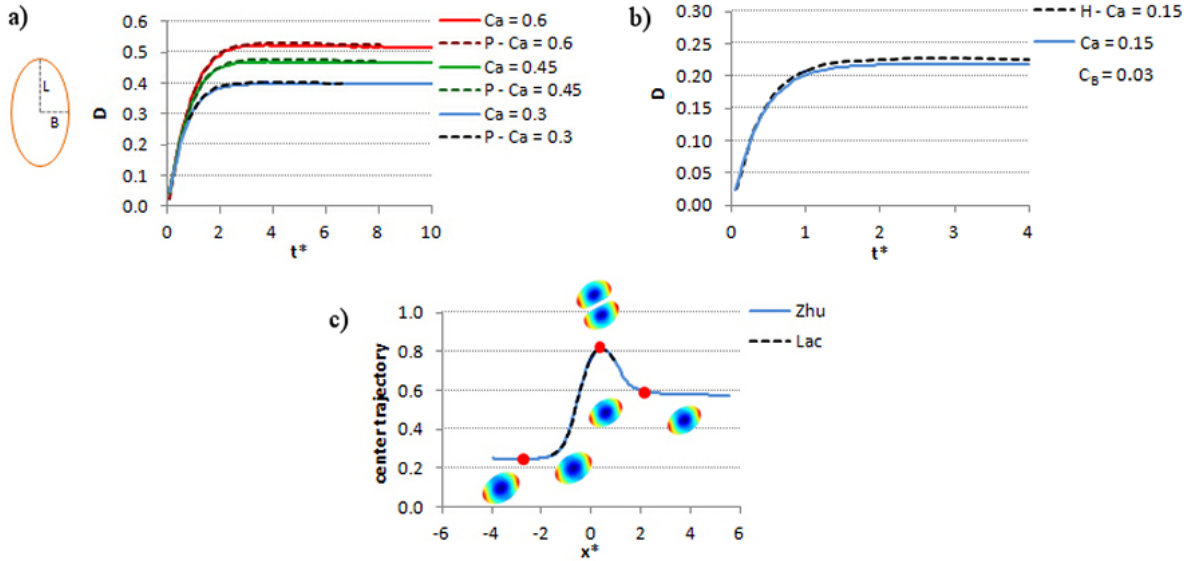


Figure 1: *a)* Deformation parameter as a function of time for single nonprestressed NH capsules in shear flow. Dotted lines are simulations from [13] and solid lines our results; *b)* Deformation parameter as a function of time for a single capsule in shear flow. Dotted lines indicate the simulations in [6], solid lines results from the present work; *c)* Vertical distance versus horizontal distance between cell centers for pair interactions. Dotted lines are simulations from Lac [9]. Solid lines from our work.

equations for inertialess flow. Finally, we validated against the results presented in Lac et al. [9]. These authors consider the hydrodynamic interaction between two pre-inflated neo-Hookean capsules under shear flow. The two capsules are slightly pre-stressed to avoid those deformation instabilities observed for a single capsule in simple shear flow in the presence of compression and negative tension. The results in Fig. 1c) display the vertical distance versus the horizontal distance of the cell centers during approach and departure. The curve obtained by our simulation perfectly matches the results in [9].

3.2 L-bend results

We report data of the deformation of a capsule passing through an L-bend. Fig. 2 shows the deformation of a capsule with capillary number $Ca = 0.15$, where the color code indicates the magnitude of the stress. The results of the first simulations clearly indicate the importance of bending stiffness as one of the governing parameters. This is very often neglected in numerical simulations of capsules and vesicles. Here we show that when flowing in bends large deformations and negative tensions easily arise. These cause bending of the membrane and can accurately be captured only including bending stiffness in the model. If this is not the case, numerical dissipation may still cure numerical instabilities but the results are then grid-dependent. To give an idea of the stress acting on a typical cell, we report also dimensional values. Assuming a flow rate of around $10\mu l/h$, and as values for the coefficients describing the cell membrane $E_S^* = 2.1 \cdot 10^{-6} N/m$ and

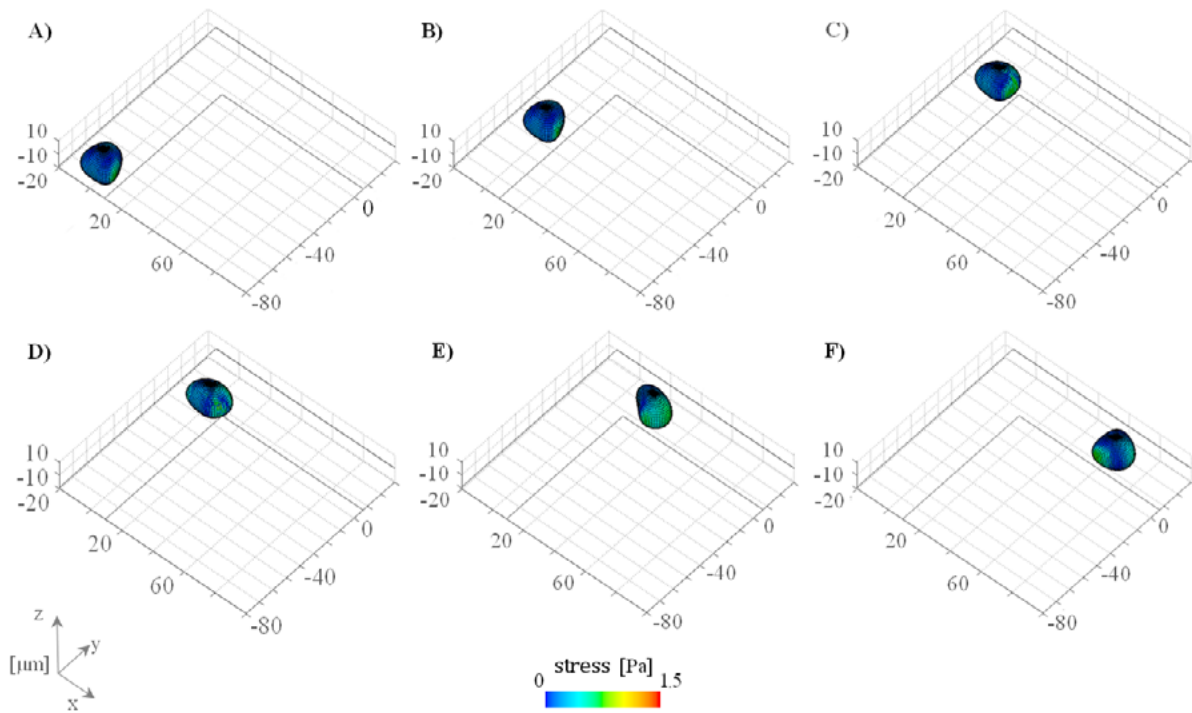


Figure 2: Capsule position in the microchannel at different instants of the simulation (A-F). Capillary number $Ca = 0.15$

$E_B^* = 1.8 \cdot 10^{-19} \text{ N} \cdot \text{m}$ [4, 18], the maximum stress experienced by the capsule is around 1.5 Pa and it increases to 5 Pa for more flexible capsules with $Ca = 0.45$.

Fig. 3 displays the area change of the capsule for three different capillary numbers: $Ca = 0.15$ (blue line), $Ca = 0.3$ (green line) and $Ca = 0.45$ (red line). The capsules with lower capillary number undergo a larger deformation in the upstream channel (initial dilation) and at the bend before recovering the original shape in the straight channel. In the lower panels in the figure one can see how the initial shape varies from bullet-type at low Capillary numbers to parachute-like for the more floppy capsules.

The same configuration is used to simulate a membrane obeying the Skalak model. Fig. 4 shows the change of total area of a capsule going through the 90-degree bend versus time for $Ca = 0.3$ and three different values of reduced area dilation modulus: $C = 1$, $C = 5$ and $C = 10$, together with a visualization of the cell shape at different positions inside the channel. For large C , i.e. large resistance to area changes, we observe lower deformations at the corner as well as a lower propagation velocity (the cell reaches the bend at a slightly later time). For $C = 1$, the cell already shows a larger area (6% higher) in the straight upstream channel that increases to about 15% around the corner.

Next we would like to compare the results for non-Hookean capsule with those for a membrane defined by the Skalak model. These models are the two most commonly used for capsules: neo-Hookean model is typically used for artificial capsules whereas

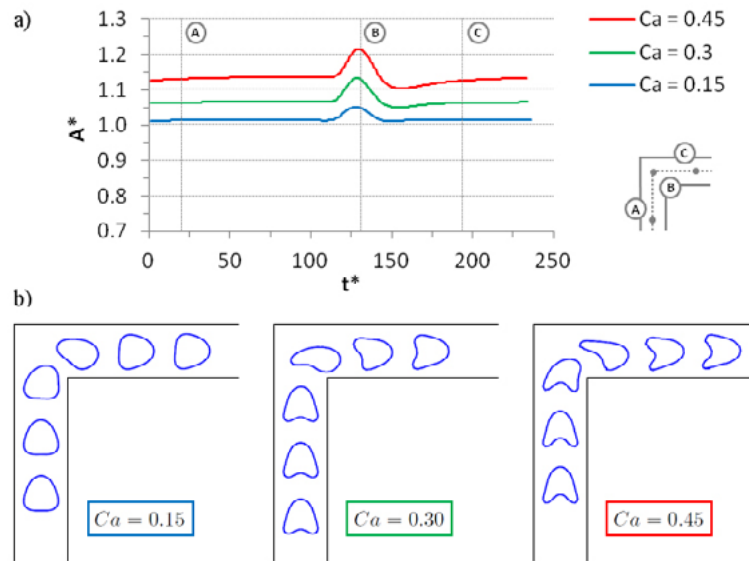


Figure 3: *a)* Area change of a capsule in motion for three cases with different capillary number: blue line $Ca = 0.15$, green line $Ca = 0.3$, red line $Ca = 0.45$; *b)* Shape change of the capsules for the three capillary numbers.

the Skalak model is used to study red blood cells. The time variation of the total area change at $Ca = 0.3$ for both models is reported in Fig. 4*a*). The capsule defined by the

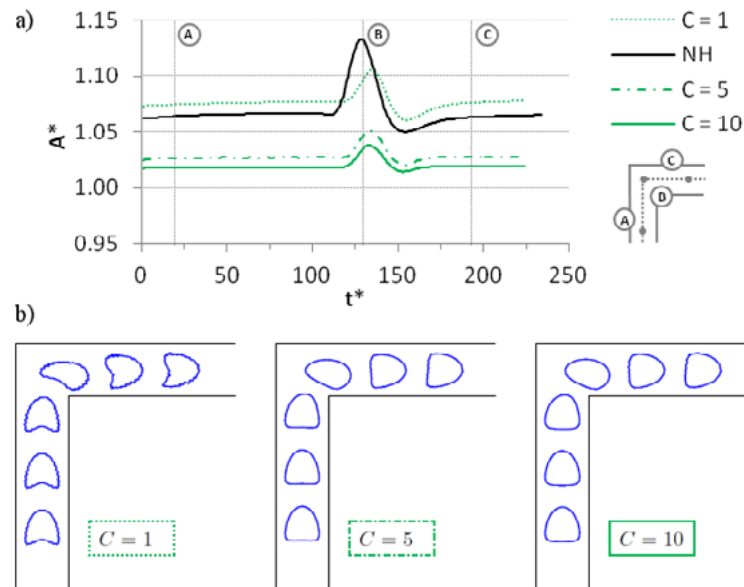


Figure 4: *a)* Area change of a capsule in motion for $Ca = 0.3$ and three different values of reduced area dilation modulus: blue line $C = 1$, green line $C = 5$, red line $C = 10$; *b)* Shape change of the capsules for the three reduced area dilation moduli.

neo-Hookean model undergoes the largest deformation at the corner, followed by a small compression in the downstream branch ($t \approx 150$). The presence of the corner is also felt earlier when there is no direct limitation on the admissible variations of the surface area.

4 CONCLUSIONS

To obtain a parametric quantification for the relations between flow rate and maximum stress/strain as well as the details of cell deformation while flowing through microfluidic chip for cell isolation highly accurate numerical simulations are necessary. Here we have presented a novel implementation of the General Geometry Ewald Method (GGEM) proposed in [13, 8] suited for realistic micro-devices.

Our simulations clearly underline the importance of bending stiffness as one of the governing parameters, very often neglected in numerical simulations. Here we show that large deformations and negative tensions easily arise, causing bending of the membrane, which can accurately be captured only including bending stiffness in the model. Therefore, this work allows us to accurately investigate cell behavior in flow in a complex geometry and to compare the behavior of different models. In the future, we plan to use our new numerical tool to optimize the design of effective micro-devices for cell isolation, where the prediction of deformation and stress acting on cell during processing is essential. Achieving this still represents one of the most significant challenges in the field of stem cells.

REFERENCES

- [1] Barthes-Biesel, D. Motion of a spherical microcapsule freely suspended in a linear shear flow. *J. Fluid Mech.*, (1980) **100(4)**:831–853
- [2] Barthes-Biesel, D. and Rallison, J.M. Time-dependent deformation of a capsule freely suspended in a linear shear flow. *J. Fluid Mech.*, (1981) **113**:251–267
- [3] Coulliette, C. and Pozrikidis, C. Motion of an array of drops through a cylindrical tube. *J. Fluid Mech.*, (1998) **358**:1–28
- [4] Evans, E.A. Bending elastic modulus of red blood cell membrane derived from buckling instability in micropipet aspiration tests. *Biophys. J.*, (1983) **43(1)**:27–37
- [5] Fischer, P.F. and Lottes, J.W. and Kerkemeier, S.G. *nek5000 Web page*, (2008) <http://nek5000.mcs.anl.gov>.
- [6] Huang, W.X. and Chang, C.B. and Sung, H.J. Three-dimensional simulation of elastic capsules in shear flow by the penalty immersed boundary method. *J. Comp. Phys.*, (2012) **231**:3340–3364
- [7] Kumar, A and Graham, M.D. Segregation by membrane rigidity in flowing binary suspensions of elastic capsules. *Phys. Rev. E*, (2011) **84**, 066316.

- [8] Kumar, A. and Graham, M.D. Accelerated boundary integral method for multiphase flow in non-periodic geometries. *J. Comp. Phys.*, (2012) **231**:6682–6713.
- [9] Lac, E. and Morel, A. and Barthes-Biesel, D. Hydrodynamic interaction between two identical capsules in simple shear flow. *J. Fluid Mech.*, (2007) **573**:149–169
- [10] Pozrikidis, C. Effect of membrane bending stiffness on the deformation of capsules in simple shear flow. *J. Fluid Mech.*, (2001) **440**:269–291
- [11] Pozrikidis, C. Numerical simulation of the flow-induced deformation of red blood cells. *Ann. Biomed. Eng.*, (2003) **31(10)**:1194–1205
- [12] Pozrikidis, C. Numerical simulation of cell motion in tube flow. *Ann. Biomed. Eng.*, (2005) **33(2)**:165–178.
- [13] Pranay, P. and Anekal, S. and Hernandez-Ortiz J. and Graham, M. Pair collisions of fluid-filled elastic capsules in shear flow: Effects of membrane properties and polymer additives. *Phys. Fluids*, (2010) **22(12)**:123103.
- [14] Sarraf, C.E. and Eastwood, M. *Topics in Tissue Engineering*. Eds. N. Ashammakhi & R.L. Reis, Vol. II. (2005).
- [15] Szita, N. and Polizzi, K. and Jaccard, N. and Baganz, F. Microfluidic approaches for systems and synthetic biology. *Curr. Opin. Biotechnol.*, (2010) **21(4)**:517–523
- [16] Yin, H. and Marshall, D. Microfluidics for single cell analysis. *Curr. Opin. Biotechnol.*, (2012) **23(1)**:110–119
- [17] Young, J.E. and Goldstein, L.S.B. Alzheimer’s disease in a dish: Promises and challenges of human stem cell models. *Hum. Mol. Genet.*, (2012) **21**:R82–R89
- [18] Zhao, H. and Isfahani, A.H.G. and Olson, L.N. and Freund, J.B. A spectral boundary integral method for flowing blood cells. *J. Comp. Phys.*, (2010) **229**:3726–3744.